On the Helical Form in Syndiotactic Poly(methyl methacrylate) Thermoreversible Gels As Revealed by Small-Angle Neutron Scattering

Alberto Saiani and Jean-Michel Guenet*

Laboratoire d'Ultrasons et de Dynamique des Fluides Complexes, Université Louis Pasteur, CNRS URA 851, 4, rue Blaise Pascal, F-67070 Strasbourg, France

Received September 17, 1996; Revised Manuscript Received December 1, 1996[⊗]

ABSTRACT: The chain trajectory within thermoreversible gels of syndiotactic poly(methyl methacrylate) (sPMMA) has been studied by small-angle neutron scattering in three solvents: chlorobenzene, bromobenzene, and toluene. It is shown that in the investigated scattering domain, the chains are rigid due to their helical conformation. Theoretical fits of the scattering curves are consistent with a double-stranded helical form in which the inner helix adopts a structure already proposed by Kusuyama et al. Just after gel melting, chains take on a new helical conformation which turns out to be more stable in chlorobenzene than in the other two solvents. The reliability of the fitting procedure is also discussed.

Introduction

Highly stereoregular poly(methyl methacrylate) forms thermoreversible gels in a large variety of organic solvents. Syndiotactic PMMA (sPMMA) and isotactic PMMA (iPMMA) can both give gels yet not necessarily in the same solvents. So far, however, investigations have been mainly focused on gels obtained from sPMMA/iPMMA mixtures probably because of the interest aroused by the formation of a so-called stereocomplex.[1−3] The helical structure involved in the stereocomplex has been well-established by Schomaker and Challa[2] and consists of a double-stranded helix, where a syndiotactic chain wraps around an isotactic filament. This is an asymmetric double helix since iPMMA takes on a 9_1 helix, whereas sPMMA adopts a 18_1 helical structure. Recent neutron scattering investigations into the gel structure have received a coherent interpretation through the use of this double helix.[3] As to iPMMA a symmetric double-stranded helix has been proposed by Tadokoro's group[4] which consists of intertwined 10_1 helices. Interestingly, the sPMMA helical structure as deduced from X-ray diffraction appears to stand as an exception. Kusuyama et al. have put forward a 74_4 single helix on the basis of results obtained on samples crystallized by solvent induction.[5] Still, the single helix has been questioned by Spěváček and co-workers[6] who have suggested the existence of a double-stranded helix instead. This conclusion is based on the reaction order of the initial stage of the self-aggregation process which turns out to be nearly 2. No well-defined structure is, however, provided for this supposedly double-stranded form. The helical conformation in sPMMA gels remains therefore a matter of debate.

The purpose of the present paper is to report on the study by small-angle neutron scattering of the chain trajectory within the gel. The results presented herein may cast some light on the helical structure involved as they favor the existence of an asymmetric double-stranded helix.

Experimental Section

1. Materials. The deuterated and the hydrogenated polymers were synthesized in toluene at −78 °C by ion-coordination polymerization with triethylaluminum and titanium(IV) chloride as catalysts.[7] In what follows they will be designated as sPMMAD and sPMMAH. It should be noted that the yield was about 40% for the hydrogenous polymer against less than 10% for the deuterated polymer.

Molecular weight characterization was performed by SEC in THF at 25 °C using the universal calibration method. The following values were obtained:

$$\text{sPMMAH} \quad M_w = 9.6 \times 10^4 \quad \text{with } M_w/M_n = 2$$

$$\text{sPMMAD} \quad M_w = 1.5 \times 10^5 \quad \text{with } M_w/M_n = 1.4$$

The tacticity of the hydrogenous polymer was determined in deuterated chloroform by means of proton NMR operating at 200 Hz. The following values were found for the tryad arrangements:

$$\text{iso} = 2\% \qquad \text{hetero} = 9\% \qquad \text{syndio} = 89\%$$

Due to the low amount of deuterated material no NMR investigation was carried out. As the thermal behavior of a 5% gel prepared from the deuterated material exhibited no significant difference compared with that of a hydrogenous polymer it was accordingly considered that stereoregularity was little altered.

2. Sample Preparation. Gel samples were prepared directly in sealable quartz cells from HELLMA of optical path of 1 mm. After sealing from atmosphere appropriate mixtures of the different consituents, the system was heated up close to the solvent boiling point so as to make clear, homogeneous solutions. Gelation was achieved by a quench to 0 °C for a minimum of 24 h. Series of gels were prepared from chlorobenzene, bromobenzene, and toluene for three global polymer concentrations: 25%, 35%, and 50% (in v/v).

Two types of sample were prepared (1) *partially-deuterated samples* containing deuterated chains imbedded in a hydrogenous gel matrix composed of sPMMAH and hydrogenated solvent and (2) *blank samples* made up with gels containing only sPMMAH and hydrogenated solvent. It is to be noted that the coherent scattering of the blank samples is negliglible so that these samples gave off mainly incoherent scattering (see Figure 1). The partially deuterated samples had a total concentration of deuterated chains of 4% and 6% (v/v), respectively.

3. Small-Angle Neutron Scattering. The experiments were carried out on PAXE small-angle camera located at the Laboratoire Léon Brillouin (LLB) (CEN Saclay, France) and on LOQ facility located at ISIS (Rutherford-Appleton Laboratory, Didcot, UK).

[⊗] Abstract published in *Advance ACS Abstracts,* February 1, 1997.

S0024-9297(96)01381-2 CCC: $14.00

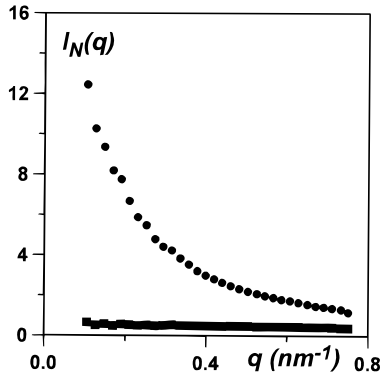

Figure 1. Comparison between the intensity scattered by a gel in which are imbedded 4% of deuterated chains (●) and a gel matrix containing only hydrogenous materials (■). In the latter case the signal is virtually flat which shows its essentially incoherent nature.

For the PAXE camera, a wavelength of $\lambda = 0.6$ nm was used with a wavelength distribution characterized by a full width at half-maximum $\Delta\lambda/\lambda_m = 10\%$. The camera possesses a two-dimensional sensitive counter composed of 128 × 128 cells (further details are available on request at LLB). By varying the sample−detector distance the available q range was in the range of $0.1 < q$ (nm^{-1}) < 2.5, with $q = (4\pi/\lambda)\sin(\theta/2)$ where θ is the scattering angle.

Counter normalization was achieved by using the incoherent scattering of hydrogenous *cis*-decalin. Typically, the normalized intensity scattered by any sample is written as

$$I_N(q) = \frac{\dfrac{I_s(q)}{T_s\delta_s} - \dfrac{I_e(q)}{T_e\delta_e}}{\dfrac{I_{dec}(q)}{T_{dec}\delta_{dec}} - \dfrac{I_e(q)}{T_e\delta_e}} \qquad (1)$$

in which I(q), δ, and T are the intensity, the thickness, and the transmission, respectively, corresponding, with the appropriate subscript, to the sample (s), to the liquid decalin (dec), and to the empty cell (e).

In order to extract the coherent intensity scattered by the deuterated chains dispersed in the hydrogenated matrix the following relation applicable to samples whose scattering is predominantly incoherent has been used:

$$I_A(q) = \frac{1}{K}\left[I_{Nd}(q) - (1 - C_p)\frac{(1 - T_d)}{T_d}\frac{T_h}{(1 - T_h)}I_{Nh}(q)\right] = M_{wp}C_pP_{pd}(q) \qquad (2)$$

in which I_{Nd} and I_{Nh} are the normalized intensities scattered by the partially deuterated sample and the matrix sample, respectively, T_d and T_h stand for their transmissions. $P_{pd}(q)$ is the form factor of the deuterated chains, C_p their concentration (expressed in g/cm^3), and M_{wp} their weight-averaged molecular weight. K is a calibration constant expressed as

$$K_{PAXE} = \frac{4\pi(a_p - y_{ps}a_m)^2\delta_{dec}T_{dec}N_A}{g(\lambda_m)(1 - T_{dec})m_p^2} \qquad (3)$$

in which a_p and a_m are the scattering amplitudes of the deuterated polymer and of the hydrogenous matrix, m_p the molecular weight of the deuterated monomer unit, y_{ps} the ratio of their molar volume (V_p/V_m). In the present case $a_m \approx 0$ for the three solvents used. $g(\lambda_m)$ is a correction factor which depends upon the neutron wavelength λ_m. Here the value of $g(\lambda_m)$ was determined by means of Cotton's method and amounts to g ($\lambda_m = 0.6$) $= 1.3 + 0.05$.

LOQ camera operates on a different principle. A burst of neutrons produced by bombarding a beryllium target is sent onto the sample. The neutron beam is not monochromatic so that time-of-flight analysis has to be performed. Once this is done the normalized intensity simply reads:[8]

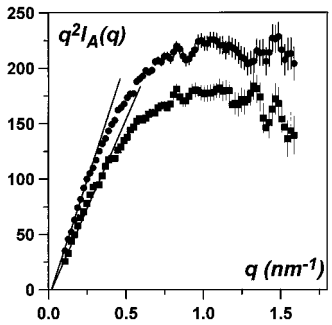

Figure 2. Intensities scattered by 6% (●) and 4% (■) chains in 35% bromobenzene gels.

$$I_N(q) = \left[\frac{I_s}{T_s} - \frac{I_B}{T_B}\right]D_c(\lambda) \qquad (4)$$

in which I and T are the scattered intensity and the transmission of the sample (s) and the empty cell (B). $D_c(\lambda)$ is a term for correcting cell efficiency. This term is known so that, unlike PAXE, normalization with an incoherent spectrum is unnecessary.

Finally, one can use relation 2 for subtracting the background. This time, however, calibration is achieved with a deuterated polystyrene standard of known molecular weight and concentration. The constant in relation 2 is accordingly written

$$K_{LOQ} = \frac{(a_p - y_{ps}a_m)^2N_A}{m_p^2} \qquad (5)$$

Note that for PAXE the normalized intensity is dimensionless, whereas it is given in centimeter^{-1} for LOQ. However, once the intensities are divided by the appropriate constants the absolute intensities are in both cases dimensionless.

For those experiments performed above room temperature. a homemade sample holder was used. It is made out of brass and heated with 10 resistors of 100 W each, regularly spaced between the apertures receiving the quartz cells. The set of resistors is controlled by a Haake TP32 temperature-monitoring device. With this setup temperature regulation turns out to be better than ±0.5 °C.

4. Calorimetry. The thermal behavior of the samples was investigated by means of a differential scanning calorimeter (DSC) from Mettler (DSC30 model). Approximately 30 mg of gel were placed in "volatile sample" pans. These pans were first heated close to solvent boiling point and then subsequently quenched to 0 °C for a minimum of 24 h and aged for a week at 20 °C. This thermal processing corresponds exactly to that employed with the "neutron" samples. The thermograms were recorded at a heating rate of 10, 5, and 2.5 °C/min.

Results and Discussion

1. Chain Trajectory in the Gel. Experiments have shown that the shape of the scattered intensity is virtually independent of the global polymer concentration. A typical result is given in Figure 2 by means of a Kratky representation ($q^2I_A(q)$ vs q). The intensities scale approximately as the deuterated polymer concentration which shows that in this q range interscattering effects may be ignored. In Figure 3 are given those data collected both on PAXE and on LOQ for 35% gels in bromobenzene and in Figure 4 for 35% gels in toluene. The different fits will be performed on these results.

The shape of the scattered intensity plotted by means of a Kratky representation is reminiscent of what was obtained by Fazel et al. on PMMA samples containing

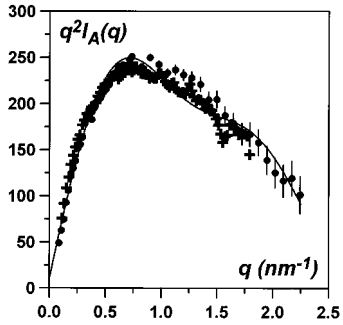

Figure 3. Intensity scattered by a 6% gel in bromobenzene (C_{pol} = 35%): ●, data from PAXE; +, data from LOQ. The solid line corresponds to the best fit (see text for details).

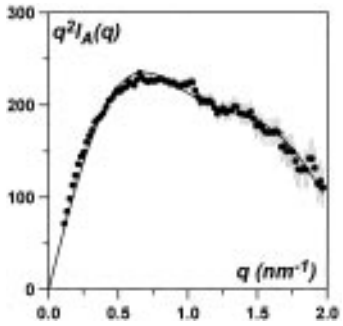

Figure 4. Intensity scattered by a 6% gel in toluene (C_{pol} = 35%). Kratky representation ($q^2I_A(q)$ vs q): data from LOQ. The solid line corresponds to the best fit (see text for details).

66% of syndiotactic triads.[3,9] These authors have shown that in these gels the polymer chains possess a *rodlike* structure due to the helicoidal conformation. Pringle and Schmitt[10] have calculated the intensity scattered by helices of infinite length characterized by an outer radius r_H and an inner radius γr_H (with $\gamma < 1$). At low resolution (for $q < 2\pi/P$ where P is the helix pitch) the intensity is written

$$q^2I_A(q) = 4\pi q C_p \mu_L \left(\frac{J_1(qr_H) - \gamma J_1(q\gamma r_H)}{qr_H(1-\gamma^2)} \right)^2 \qquad (6)$$

in which μ_L is the mass per unit length of the helix and J_1 the Bessel function of first kind and first order. This relation turns out to be the same as that calculated for a hollow cylinder.[11] As a rule the intensity can be written independent of the cross section

$$q_2I_A(q) = \pi q C_p \mu_L f(qR_\sigma) + \text{Cte} \qquad (7)$$

in which R_σ is the radius of gyration of the cross section and Cte a constant term taking into account interscattering effects. For $qR_\sigma < 1$ relation 7 reduces to

$$q_2I_A(q) = \pi C_p \mu_L q \exp -q^2 R_\sigma^2/2 \qquad (8)$$

In the case of the helical form described by relation 6, the cross section radius of gyration is related to the outer radius through

$$R_\sigma^2 = \frac{r_H^2(1+\gamma^2)}{2} = \frac{r_H^2(2 - 2e/r + e^2/r^2)}{2} \qquad (9)$$

in which e is the "thickness" of the helix ($e = r_H - \gamma r_H$). In the case of sPMMA this "thickness" corresponds approximately to the chain diameter under an all-extended conformation.[12] R_σ can be determined by a

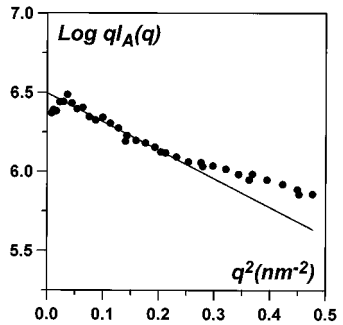

Figure 5. Intensity scattered by a 6% gel in bromobenzene (C_{pol} = 35%) plotted by means of a Porod plot (log $qI_A(q)$ vs q^2); data from PAXE. The solid line corresponds to the linear regime.

Porod plot, that is by plotting log $qI_A(q)$ vs q^2. The Porod plot is another way of checking that the scattered intensity is of the type given by relation 7. Such a plot is drawn in Figure 5. A cross section radius of gyration of $R_\sigma = 1.9 \pm 0.2$ nm is derived from the linear slope seen at small q.

So far the only helical form proposed by Kusuyama et al.[5] for sPMMA consists of a 74_4 helix of fiber period = 3.54 nm, with outer and inner radii of $r_H \simeq 1.0$ nm and $\gamma r_H \simeq 0.5$ nm, respectively. For such a helix $R_\sigma \simeq 0.79$ nm which is at variance with the experimental value found here. Clearly, Kusuyama et al.'s helical form cannot be used as such to account for the scattering curve. One has to consider either another single helix with a larger radius or two helical forms. In the case of a single helix the outer radius ought to be of about 2 nm as derived from relation 9. The pitch P can be estimated from the experimental mass per unit length and the mass per unit length μ_o, corresponding to the contour length of the PMMA chain. As the sPMMA chain is liable to take on locally a *tt* arrangement[12] this yields $\mu_o \approx 390$ g/(mol nm). The pitch is then expressed through

$$P^2 = \frac{4\pi^2 r_{mid}^2}{(\mu_L/\mu_o)^2 - 1} \qquad (10)$$

in which $r_{mid} = (r_H + \gamma r_H)/2$. Relation 10 gives a pitch of about 1.4 nm, i.e. about 40 monomers/turn (monomers/turn = $P\mu_L/108$). The polymer density within the ring of such a helix would amount to 1.7 g/cm^3 which seems to be rather unrealistic. We shall therefore explore the case with two helices which, as will be seen, offers the advantage of incorporating Kusuyama et al.'s helical form. We shall rather consider a double helix as already suggested by Spěváček.[6] A double helix is contemplated because it is easier to justify from a thermodynamic viewpoint. If the system is at equilibrium or near equilibrium two domains constituted with different kinds of helices cannot coexist in a wide range of concentrations without violating Gibbs phase rule.

Admittedly, one helix can be metastable and form faster than the stable one at high undercoolings so that two populations can be present at the same time. Although the metastable helix should transform into the stable form they may coexist over a certain period of time. The cooling rate at which the gel is produced is therefore a key parameter. Slow cooling rates should produce the stable helix only, whereas high cooling rates should favor the growth of the metastable form. No

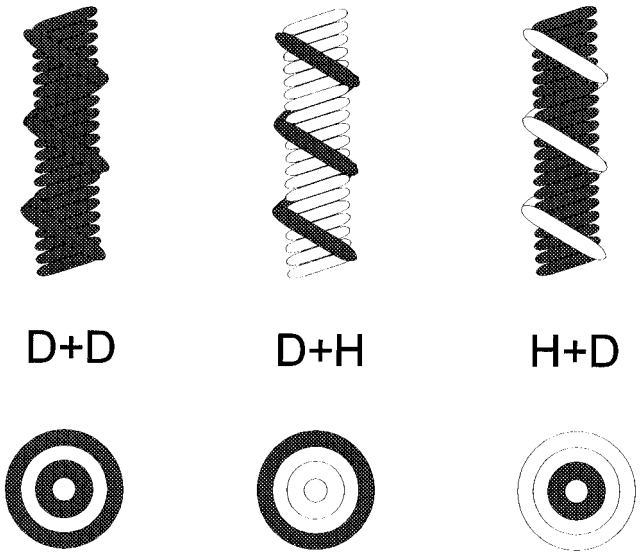

Figure 6. Schematic representation of an asymmetric double-stranded helix. Black and white mimic the different labeling. Rings located below portray the equivalent cross section at low resolution.

noticeable effects on the gel properties nor on the scattering curve were seen by varying this parameter so that a mixture of stable and metastable helical forms should be discarded.

When dealing with double helices three labeling cases as drawn in Figure 6 have to be taken into account: only the outer helix is labeled, only the inner helix is labeled, and both helices are labeled. For the first two cases the scattered intensity is given by relation 6 since the protonated helix does not give off any coherent scattering. For the third case a new relation is derived by considering two coaxial hollow cylinders of infinite length as permitted by the level of resolution:[13]

$$q^2 I_A(q) \sim \pi q \left[\frac{\int_{\gamma_1 r_1}^{r_1} 2\pi r J_o(qr)\, dr + \int_{\gamma_2 r_2}^{r_2} 2\pi r J_o(qr)\, dr}{\int_{\gamma_1 r_1}^{r_1} 2\pi r\, dr + \int_{\gamma_2 r_2}^{r_2} 2\pi r\, dr} \right]^2 \tag{11}$$

Performing the integrations finally gives

$$q^2 I_A(q) \sim 4\pi q C_p \mu_{L12} \left(\frac{r_1 J_1(qr_1) - \gamma_1 r_1 J_1(q\gamma_1 r_1) + r_2 J_1(qr_2) - \gamma_2 r_2 J_1(q\gamma_2 r_2)}{q r_1^2 (1 - \gamma_1^2) + q r_2^2 (1 - \gamma_2^2)} \right)^2 \tag{12}$$

with

$$\mu_{L12} = \mu_{L1} + \mu_{L2} \tag{13}$$

and in which the subscripts 1 and 2 stand for the inner helix and the outer helix, respectively.

The intensity scattered by the deuterated chains is written

$$I_A(q) \sim W_{12} I_{A12}(q) + W_1 I_{A1}(q) + W_2 I_{A2}(q) \tag{14}$$

in which W and $I_A(q)$, with the appropriate subscript, are the weight fraction of each of the three possible cases and the corresponding intensity, respectively. Again the case H + H is ignored as its coherent scattering is negligible. These weight fractions can be expressed as follows:

$$W_{12} = \frac{P_{12}(\mu_{L1} + \mu_{L2})}{P_{12}(\mu_{L1} + \mu_{L2}) + P_1 \mu_{L1} + P_2 \mu_{L2}} = \frac{P_{12}}{P_{12} + P_2} \tag{15}$$

in which P and μ_L, with the appropriate subscripts, are the probabilities and the mass per unit length for each case. Similarly, one obtains for W_1 and W_2

$$W_2 = \frac{P_2}{P_{12} + P_2} \frac{\mu_{L2}}{\mu_{L2} + \mu_{L1}}$$
$$W_1 = \frac{P_1}{P_{12} + P_2} \frac{\mu_{L1}}{\mu_{L2} + \mu_{L1}} \tag{16}$$

These probabilities are calculated by means of combinatorial analysis assuming infinitely long chains. If there are N_D deuterated chains and N_H hydrogenated chains, then the probability for finding a double helix totally deuterated is

$$P_{12} = C_{N_D}^{\ 2} / C_{N_D + N_H}^{\ 2} \tag{17}$$

while the probability for having only one deuterated chain in the double helix is

$$P_1 = P_2 = {}^1/_2 (C_{N_D}^{\ 1} C_{N_H}^{\ 1}) / C_{N_D + N_H}^{\ 2} \tag{18}$$

in which $C_n^p = n!/p!(n-p)!$. The different probabilities can be calculated for large number of chains by using Stirling formula $n! = (2\pi n)^{1/2} n^n e^{-n}$. For the experimental case shown in Figure 3, that is 6% deuterated samples for a polymer concentration of 35%, 17 chains out of 100, approximately, are deuterated. The probabilities tend to the following values for n large: $P_{12} = 0.029$ and $P_1 = P_2 = 0.14$. Note that the sum of these probabilities is not 1 because the case where both chains are hydrogenated is not considered. The case where both helices are labeled for $C_D = 6\%$ amounts to about 10% of the coherently scattering species, a fact which cannot be disregarded.

In Figure 3 is shown the best fit obtained through relation 14 for all the experimental points. This fit uses four parameters of which the most important are the two different radii since they determine the shape of the scattering curve. The fitting procedure carried out with MicroCal ORIGIN provided one with the following values:

radius of the inner helix
$r_1 = 1.1 \pm 0.2$ nm $\quad \mu_{L1} = 2410 \pm 300$ g/(mol nm)

radius of the outer helix
$r_2 = 2.3 \pm 0.3$ nm $\quad \mu_{L2} = 1580 \pm 200$ g/(mol nm)

Before proceeding further in the discussion of these data it is worth mentioning that R_σ can be calculated from

$$R_\sigma^2 = \frac{1}{2\mu_L} \left[W_{12}(\mu_{L1} + \mu_{L2}) \frac{r_1^4 (1 - \gamma_1^4) + r_2^4 (1 - \gamma_2^4)}{r_1^2 (1 - \gamma_1^2) + r_2^2 (1 - \gamma_2^2)} + W_1 \mu_{L1} r_1^2 (1 + \gamma_1^2) + W_2 \mu_{L2} r_2^2 (1 + \gamma_2^2) \right] \tag{19}$$

in which

$$\mu_L = W_{12}(\mu_{L1} + \mu_{L1}) + W_1\mu_{L1} + W_2\mu_{L2} \qquad (20)$$

From the above radii obtained through the fit of the entire scattering curve, relation 19 yields $R_\sigma = 1.7 \pm 0.2$ nm, a value in good agreement with that obtained from the Porod plot (in Figure 4).

Interestingly, the radius of the inner helix as well as the mass per unit length correspond within experimental uncertainties to the helix proposed by Kusuyama et al. ($\mu_K = 2260$ g/(mol nm) for deuterated chains). The outer helix appears to be significantly more extended as the pitch is $P_{outer} \approx 3.5$ to 4 nm against $P_{inner} \approx 0.9$ nm for the inner helix. Here we shall emphasize that more refined models that incorporate the possible presence of amorphous material could probably improve the fit. Examples will be discussed in the forthcoming section. Only diffraction experiments are liable to provide one with more precise values of the pitch. It is, however, worth realizing that the *a* and *b* parameters of the crystalline lattice proposed by Kusuyama et al.[5] ($a = b = 4.35$ nm) would be consistent with a close packing of such double helices.

The fit of the scattering curves therefore suggests the existence of another helical form that wraps around the structure proposed by Kusuyama et al. A symmetrical double helix (two helices of same pitch) should be dismissed as the mass per unit length of the outer strand ought to be about 5000 g/(nm mol), a figure beyond the limits that the theoretical fit would allow. Admittedly, asymmetric double helices are uncommon as are, incidentally, helical forms as Kusuyama's. One example of an asymmetric double-stranded helix is the iPMMA/sPMMA stereocomplex, but here the chemical arrangements of the monomers differ for each strand. Interestingly, however, is that sPMMA in the stereocomplex structure takes on a helical form which significantly differs from Kusuyama's (the latter contains about twice the number of monomers per axial rise than the former). This does indicate that while the local conformation is *tt*, sPMMA is liable to produce different helical forms. The case of an irregular outer helix should also be contemplated.

Several authors have reported that gelation of sPMMA occurs in two marked steps.[1,14] The first step corresponds to a rapid conformational change and the second one to chain aggregation. One may wonder whether these two steps are related to the asymmetry of the double helix considered here: first formation of Kusuayma's form followed by the wrapping of the outer helix around?

Finally, it is worth pointing out that the different radii deduced from the fit imply a gap between the two helices of about 0.7 nm. As was shown by Kusuyama et al., their helix is probably solvated with some of the solvent molecules pointing outward. A solvent molecule of the type used here could be responsible for that gap as their length is of about 0.5 nm. The outer helix would then wrap around a solvated helix.

2. Chain Trajectory vs Temperature. The investigation of the chain trajectory as a function of temperature has been limited to 35% gels. Typical melting endotherms recorded at 10 °C/min are shown in Figure 7. Careful determination of all the actual temperature at which the thermal events of interest occur has been achieved by varying the heating rate. As can be seen, gels prepared from bromobenzene and toluene display only one melting endotherm unlike those from chlorobenzene. In the latter case a second endotherm can be observed (the temperature−concentration phase diagramm will be reported in due course). In the case of toluene and bromobenzene, the neutron scattering experiments have been carried out just after gel melting as determined by extrapolatation to zero-heating rate. Concerning gels in chlorobenzene, neutron data have been collected just after the first endotherm, after the terminal melting and at various temperatures up to a few degrees below the solvent boiling point (see figure captions for details).

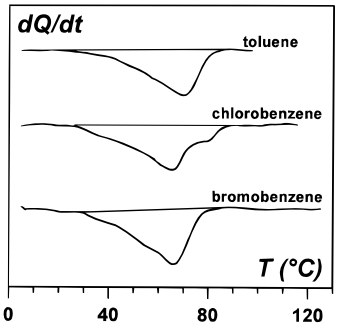

Figure 7. DSC traces obtained at 10 °C/min for the different 35% gels. Solvents as indicated.

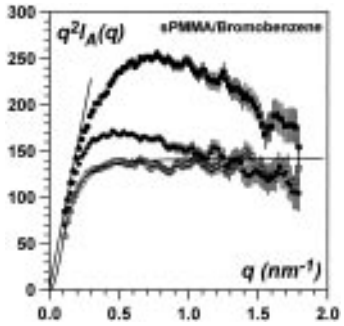

Figure 8. Intensity scattered by a 6% gel in bromobenzene ($C_{pol} = 35\%$). Kratky representation ($q^2I_A(q)$ vs q); data from LOQ: ●, room temperature; ◆, temperatures from 77 °C to 85 °C; ○, $T = 145$ °C. (Boiling point of bromobenzene $T_B = 156$ °C.) Solid line stands for the fit by means of a Debye function (see text for details).

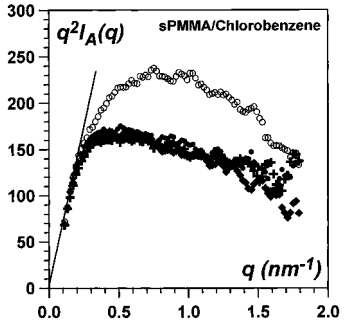

Figure 9. Intensity scattered by a 6% gel in chlorobenzene ($C_{pol} = 35\%$). Kratky representation ($q^2I_A(q)$ vs q); data from LOQ: ○, room temperature; ◆, 67 °C; +, 70 °C; ●, 126 °C. (Boiling point of chlorobenzene $T_B = 132$ °C.)

The results are reported in Figure 8 for bromobenzene, Figure 9 for chlorobenzene, and Figure 10 for toluene. For the temperatures investigated two steps are apparent in chlorobenzene and bromobenzene unlike in toluene. There is a significant change just after gel melting yet the resulting chain conformation (conformation II) is kept over a wide domain of temperature. At higher temperature, in particular close to the solvent boiling point, another chain conformation (conformation III) shows up in bromobenzene and toluene. In chlorobenzene, conformation II is observed throughout the

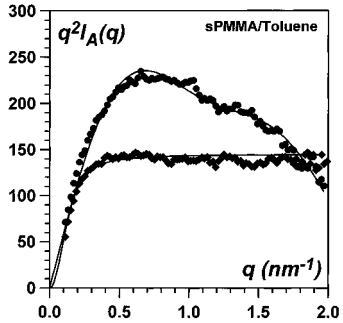

Figure 10. Intensity scattered by a 6% gel in toluene (C_{pol} = 35%). Kratky representation ($q^2I_A(q)$ vs q); data from LOQ: ●, room temperature; ◆, 106 °C. (Boiling point of toluene T_B = 110 °C.)

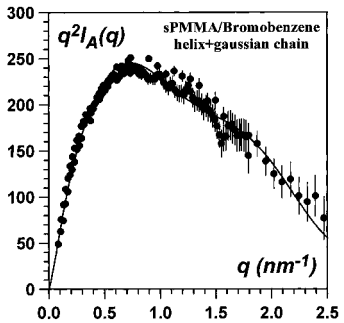

Figure 11. Intensity scattered by a 6% gel in bromobenzene (C_{pol} = 35%): data from PAXE and LDQ. The solid line corresponds to the best fit obtained by considering the presence of 30% of Gaussian chains (see text for details).

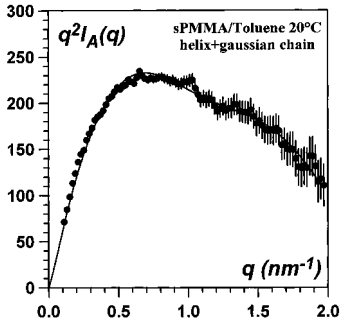

Figure 12. Intensity scattered by a 6% gel in toluene (C_{pol} = 35%). The solid line corresponds to the best fit obtained by considering the presence of 20% of Gaussian chains (see text for details).

domain of temperature investigated. This suggests that conformation II obtained just after gel melting is more stable in chlorobenzene than in the other two solvents. Interestingly, conformation II can exist both in the sol state (in chlorobenzene or in bromobenzene) but also in an organized state in chlorobenzene.

The behavior observed in bromobenzene and toluene at high temperature is manifestly of the type $I(q) \approx q^{-2}$. Conformation III is therefore Gaussian whose scattering function is given to a good approximation by the so-called Debye function:

$$I_A(q) = C_p M_w \frac{2}{q^4 R_G{}^4}[\exp -q^2 R_G{}^2 - 1 + q^2 R_G{}^2] \quad (21)$$

in which R_G is the mean-square radius of gyration and M_w the weight-averaged molecular weight. This function provides a very good fit of the experimental scattering function although no correction for polydispersity has been taken into account as this parameter is rather low for the deuterated chains used in this study. The following values are obtained: $R_G = 10.1$ nm and $M_w = 9.5 \times 10^4$ in bromobenzene and $R_G = 9.9$ nm and $M_w = 9.2 \times 10^4$ in toluene. The value found for the weight-averaged molecular weight agrees reasonably well with that obtained by SEC keeping in mind that both techniques are subject to calibration procedures, and also that in this q range the fit is likely to give an averaged molecular weight closer to the number-averaged molecular weight.[15] The radius of gyration corresponds to what is known for atactic PMMA in good solvents.[16]

With regard to conformation II obtained just after gel melting, models made up with a mixture of Gaussian chains and helix (either the double helix considered here or Kusuyama's helix) have failed to reproduce the experimental data. The fact that this conformation exists in an organized state in chlorobenzene points toward another helical form. Clearly, additional data are required for elucidating this conformation.

Despite the absence of a suitable model to account for the neutron data after gel melting, the body of the results highlight a melting process different from that observed with chain-folded crystals where the chains recover virtually instanteneously their Gaussian conformation.[17] Here some stabilization process prevents them from doing so which appears to be solvent-dependent: chlorobenzene appears to stabilize to a better extent this conformation. This is reminiscent of conclusions already reached for polystyrene (isotactic or syndiotactic). This may suggest that solvent housing between the ester groups is also a stabilization process worth contemplating for sPMMA systems.[18]

Table 1. Different Parameters Obtained by a Fit of the Scattering Curves[a]

solvent	outer radius	inner radius	μ_{outer}	μ_{inner}
pure helix	2.3 ± 0.3	1.1 ± 0.2	1580 ± 200	2410 ± 300
helix + Gaussian (toluene)	2.5 ± 0.3	1.2 ± 0.2	1600 ± 200	2750 ± 200
helix + Gaussian (bromobenzene)	2.3 ± 0.3	1.1 ± 0.2	1760 ± 200	2870 ± 300

[a] Radii are given in nm and mass per unit length (μ) in g/(mol nm). The first row stands for the values derived by considering a pure double helix. Rows 2 and 3 are the values found by considering a mixture of double helices and Gaussian chains.

3. A Critical Evaluation of the Fitting Procedure. So far the scattering curve fitting has been performed by considering a pure double-helix model. One may wonder at the degree of confidence that can be granted to this approach. To test the reliability of the fit, in particular on the values of the different cross section radii and masses per unit length, a more complex model has been considered which relies upon experimental findings by Spěváček and co-workers.[19,20] These authors have shown by NMR measurements that a fraction of the polymer is not engaged in the gelation process which amounts to about 20% in toluene[19] and to 30% in bromobenzene.[20] This fraction possibly consists in less stereoregular chains that cannot take on the appropriate helical form to be incorporated into the gel structure. A more complex model consists therefore of considering a mixture of double helices and Gaussian chains. For the latter, it is assumed that they adopt a Gaussian statistics whose parameters are those determined by the fits at high temperature. The fractions of these gaussian chains correspond to those reported by Spěvàček and co-workers. The only varying

parameters are again the cross section radii and the mass per unit length. In so doing a much better fit is obtained as can be seen in Figures 11 and 12. More interesting, however, is that there is no significant difference as far as the helical cross-section radii are concerned as is apparent from Table 1. The only noticeable discrepancy is found for the values of the mass per unit length which highlights their lesser reliability.

Concluding Remarks

The results presented here together with their interpretation suggest the occurrence in sPMMA gels of a double-stranded helical form, displaying strong asymmetry with one of the strands close to the helical form proposed by Kusuyama et al.[5] In addition, this double helix is consistent with the lattice parameters as proposed by the same authors. It remains to elucidate the role of the solvent, and particularly its precise location within the structure. Experiments carried out as a function of temperature and solvent type clearly indicate that this is an important parameter for understanding thermoreversible gelation of sPMMA.

Acknowledgment. The authors are greatly indebted to Dr. S. M. King from Rutherford-Appleton Laboratory and to Dr. A. Brûlet from Laboratoire L. Brillouin for experimental assistance as well as to O. Gavat for the synthesis of the sPMMA samples.

References and Notes

(1) See for a review: Spěváček, J.; Schneider, B. *Adv. Coll. Interface Sci.* **1987**, *27*, 81.
(2) Schomaker, E.; Challa, G. *Macromolecules* **1989**, *22*, 3337.
(3) Fazel, N.; Brûlet, A.; Guenet, J. M. *Macromolecules* **1994**, *27*, 3836.
(4) Kusunagi, H.; Tadokoro, H.; Chatani, Y. *Macromolecules* **1976**, *9*, 531.
(5) Kusuyama, H.; Miyamoto, N.; Chatani, Y.; Tadokoro, H. *Polym. Commun.* **1983**, *24*, 119.
(6) Dybal, G.; Spěváček, J.; Schneider, B. *J. Polym. Sci. Polym. Phys. Ed.* **1986**, *24*, 657.
(7) Abe, H., Imai, K.; Matsumoto M. *J. Polym. Sci. Part C* **1968**, *23*, 469.
(8) Heenan, R. K.; King, S. M. *Proceedings International Seminar on Structural Investigation at Pulsed Neutron Sources*; Aksenov, V. L., Balagerov, A. M., Taran, Yu. V., Eds.; JINR: Dubna, 1992.
(9) Fazel, N.; Fazel, Z.; Brûlet, A.; Guenet, J. M. *J. Phys. II* **1992**, *2*, 1617.
(10) Pringle, O. A.; Schmidt, P. W. *J. Appl. Crystallogr.* **1971**, *4*, 290.
(11) Oster, G.; Riley, D. P. *Acta Crystallogr.* **1952**, *5*, 272.
(12) Lovell, R.; Windle, A. H. *Polymer* **1981**, *22*, 175.
(13) Mittelbach, P.; Porod, G. *Acta Phys. Aust.* **1961**, *14*, 405.
(14) Berghmans, H.; Donkers, A.; Frenay, L.; De Schryver, F. E.; Moldanaers, P.; Mewis, J. *Polymer* **1987**, *28*, 97.
(15) Benoit, H. *J. Polym. Sci.* **1953**, *11*, 507.
(16) See for instance: Kirste, R. G.; Schulz, G. V. *Z. Phys. Chem.* **1961**, *30*, 171. Katime, I.; Roig, A.; Leon, L. M.; Montero, S. *Eur. Polym. J.* **1977**, *13*, 59.
(17) Barham, P. J. *Crystallization of Polymers* Dosiere, M., Ed.; Kluwer Academic: Dordrecht, 1993, p 153.
(18) Guenet, J. M. *Thermoreversible Gelation of Polymers and Biopolymers*; Acad. Press: London, 1992.
(19) Spěváček, J.; Schneider, B.; Bohdanecky, M.; Sikora, A. *J. Polym. Sci. Polym. Phys. Ed.* **1982**, *20*, 1623.
(20) Spěvàček, J. Private communication.

MA961381X